Earth and Planetary Science Letters 554 (2021) 116675

Contents lists available at ScienceDirect

Earth and Planetary Science Letters

www.elsevier.com/locate/epsl

Regional patterns and temporal evolution of ocean iron fertilization and CO_2 drawdown during the last glacial termination

Fabrice Lambert [a,*], Natalia Opazo [a], Andy Ridgwell [b], Gisela Winckler [c], Frank Lamy [d], Gary Shaffer [e,f], Karen Kohfeld [g,h], Rumi Ohgaito [i], Samuel Albani [j], Ayako Abe-Ouchi [k]

[a] Department of Physical Geography, Pontifical Catholic University of Chile, Chile
[b] Department of Earth and Planetary Sciences, University of California, Riverside, USA
[c] Lamont-Doherty Earth Observatory of Columbia University, Palisades, New York 10964, USA
[d] Alfred-Wegener-Institut Helmholtz-Zentrum für Polar- und Meeresforschung, 27570 Bremerhaven, Germany
[e] Research Center GAIA Antarctica, University of Magallanes, Chile
[f] Niels Bohr Institute, University of Copenhagen, Denmark
[g] School of Resource and Environmental Management, Simon Fraser University, Canada
[h] School of Environmental Science, Simon Fraser University, Canada
[i] Japan Agency for Marine-Earth Science and Technology, Yokohama, 236-0001, Japan
[j] Department of Environmental and Earth Sciences, Università degli Studi di Milano-Bicocca, Italy
[k] Atmosphere Ocean Research Institute, University of Tokyo, Kashiwa, Chiba 277-8564, Japan

ARTICLE INFO

Article history:
Received 27 February 2020
Received in revised form 5 September 2020
Accepted 8 November 2020
Available online 27 November 2020
Editor: L. Robinson

Keywords:
CO_2
dust
iron fertilization
paleoclimate
termination

ABSTRACT

The last time Earth's climate experienced geologically rapid global warming was associated with the last glacial termination, when atmospheric CO_2 concentrations rose from 180 ppmv during the Last Glacial Maximum (LGM, 26-19 kaBP) to ~260 ppmv by the early Holocene (12-8 kaBP). About one quarter of that difference is thought to be due to a stronger biological pump during glacial times, driven by increased aeolian dust deposition and hence greater iron availability in ocean surface waters. However, dust supply did not change uniformly or in synchrony over the deglacial transition and what is not known is the relative importance of different oceanic regions and how this may have changed in time. Using an Earth system model of intermediate complexity, we quantify the sensitivity of atmospheric CO_2 to regional changes in iron supply, and test six different global dust reconstructions in order to explore uncertainty in past dust changes. We confirm the Southern Ocean (>34°S) as the region most sensitive to iron fertilization, with the Atlantic and Pacific sectors accounting for about 41±23% and 16±10%, respectively, of the total CO_2 reduction from global iron fertilization. However, the North Pacific contributes 28±3% to the total implying an important role for Northern Hemisphere processes in driving deglacial CO_2 rise. In addition, our analysis reveals an unexpected regional-temporal disparity, and while Southern Hemisphere iron fertilization influences atmospheric CO_2 relatively constantly throughout the termination the impact of the Northern Hemisphere only occurs during the later stages of the termination.

1. Introduction

Over the last 800,000 years Earth's climate has alternated between cold glacial and warm interglacial stages (Jouzel et al., 2007; Lisiecki and Raymo, 2005), with global temperature and atmospheric CO_2 variations being intrinsically linked in a strong linear relationship (Fischer et al., 2010), (Bereiter et al., 2015). Atmospheric CO_2 is hence thought to be one of the main internal feedback mechanisms of Earth's climate system for large-scale climatic change (Chowdhry Beeman et al., 2019; Shakun et al., 2012). Understanding the cause of the variations in CO_2, which during the last 800,000 years were lower during glacials (170-190 ppmv) than during interglacials (250-300 ppmv) (Bereiter et al., 2015), is thus central to understanding glacial-interglacial climates variability as a whole.

Mineral dust aerosols also influence climate through radiative processes such as absorption and scattering of photons (Tegen et al., 1996), and modification of cloud properties (Lohmann and Feichter, 2005), as well as through their impact on biogeochemistry (Martin et al., 1991; Tagliabue et al., 2017). Their atmospheric abundance changes through the glacial-interglacial cycles, and higher atmospheric dust concentrations during glacial times

* Corresponding author.
E-mail address: lambert@uc.cl (F. Lambert).

https://doi.org/10.1016/j.epsl.2020.116675

may have helped cool climate by up to one third of the glacial maximum-interglacial temperature difference through scattering of solar radiation and lowering of atmospheric CO_2 concentrations through iron fertilization (IF) of the oceans (Shaffer and Lambert, 2018). However, unlike greenhouse gases, dust deposition fluxes appear to be exponentially linked to temperature and CO_2 changes (Lambert et al., 2008; Ridgwell, 2003; Shaffer and Lambert, 2018), with dust values remaining low for much of the early glacial stages but reaching maximum deposition during glacial maxima (Lambert et al., 2008; Lamy et al., 2014; Pourmand et al., 2004; Serno et al., 2015). The sharp reduction in atmospheric dust concentrations during glacial-interglacial transitions may therefore have had a significant impact on CO_2 and temperature (Watson et al., 2000).

Why atmospheric CO_2 was lower during glacial times is understood in principle (Fischer et al., 2010). At the LGM atmospheric CO_2 concentrations were 80-100 ppmv lower than during the Holocene (Bereiter et al., 2015). A large fraction of this difference (40-50 ppmv) is thought to be due to increased glacial oceanic stratification and subsequent accumulation of CO_2 in the deep ocean layers (Francois et al., 1997). Another 20 ppmv may be due to stimulation of ocean surface biological activity through micronutrient supply by mineral dust particles (Köhler and Fischer, 2006; Lambert et al., 2015). The sum of various additional processes (sea-ice cover, terrestrial biosphere carbon storage, ocean salinity and temperature, remineralization depth, ocean carbonate compensation, non-aeolian iron sources) likely accounts for the rest (Chikamoto et al., 2012; Fischer et al., 2010; Sigman and Boyle, 2000; Tagliabue et al., 2017). Although numerous studies have created proxy-based constraints on past marine productivity (Anderson et al., 2014; Chase et al., 2003; Kohfeld and Chase, 2011; Lamy et al., 2014; Pourmand et al., 2004) and CO_2 outgassing from the ocean (Martínez-Botí et al., 2015), these records only show the sum of all processes that affect productivity and CO_2 exchanges in that place and parsing out the global atmospheric CO_2 impacts from carbon cycle changes occurring at individual sites or regions is challenging.

The mechanism by which a reduction of atmospheric CO_2 can occur through increased dust deposition, is an intensification of the biological pump (Hain et al., 2014). Some regions of the world's ocean are rich in macronutrients (e.g. phosphate, nitrate) but depleted in the micronutrient iron, inhibiting biological growth (the so-called High Nutrient Low Chlorophyll -HNLC- regions, Fig. 1) (Martin et al., 1991). Higher dust deposition in these regions during glacial times is thought to have increased soluble iron content in ocean surface waters. This enhanced biological productivity and improved the efficiency of the biological pump, thereby increasing the transfer of CO_2 from the atmosphere to the deep ocean (Martin et al., 1991; Tagliabue et al., 2017). Current estimates of increased dust deposition during glacial times on ocean biogeochemistry cycles point to the Southern Ocean (the largest HNLC region) and the South American dust sources (the strongest LGM dust source in the Southern Hemisphere) as the main drivers of the IF effect during the LGM (Costa et al., 2016; Lambert et al., 2015; Shoenfelt et al., 2018; Yamamoto et al., 2019).

However, the last glacial termination was characterized by a complex time-varying pattern of CO_2 change, providing clues to the key processes but also challenges to interpretation. The deglacial CO_2 rise occurred mainly in two periods, one pulse of 32 ppmv from 17.4-16.2 kaBP before the Atlantic Cold Reversal (ACR), and another pulse of 32 ppmv just after the ACR from 13.2 to 11.5 kaBP (yellow bars in Fig. 2). These two pulses are generally associated with 'de-stratification' events in the ocean that would have brought CO_2-rich deep ocean waters to the surface (Martínez-Botí et al., 2015; Monnin et al., 2001). Upwelling deep water would also have been rich in nutrients and would have produced a surge in biological activity. Opal measurements in marine sediment cores are generally interpreted as indicators of such events, but the regional heterogeneity of even the sign of productivity change between the LGM and the Holocene (Fig. 1) suggests a very complex spatial and temporal evolution of the marine carbon cycle, with local circulation changes having a strong influence (Kohfeld et al., 2013, 2005; Kohfeld and Chase, 2011). In addition, changes in dust flux and hence the contribution of IF to changing atmospheric CO_2 is also both spatially and temporally heterogeneous —a product of regional land surface dynamics in dust source regions together with atmospheric circulation patterns. Indeed, Southern Hemisphere dust fluxes appear to have changed mostly during the older CO_2 pulse, while Northern Hemisphere dust seems to have stayed at high levels until the younger pulse (Fig. 2b and 2e).

Here, we aim to de-convolve the complex spatially and temporally varying contribution of IF to atmospheric CO_2 rise since the last glacial maximum, and deliberately quantify the iron fertilization from aeolian origin in isolation from any other physical (e.g. ocean destratification, sea-ice, temperature) or biogeochemical effect taking place. Using a range of simulated and measured global paleoclimatic dust flux datasets, we investigate the effect of reduced dust fluxes to specific ocean surface areas on atmospheric CO_2 during the last glacial termination (20-10 kaBP). In addition, we investigate the temporal relationship between dust deposition and atmospheric CO_2 during the last glacial termination for the main HNLC regions.

2. Methods

2.1. Geographical regions

We considered 4 main HNLC regions (Martin et al., 1991): The Southern Ocean comprising the South Atlantic and Indian (SAI; 34S, 70W–90S, 150E) and South Pacific (SP; 34S, 150E–90S, 70W) sectors, the North Pacific (NP; 90N, 120E – 34N, 110W), and the Central East Pacific (CEP; 6S, 170W–6N, 80W) (Fig. 1). The Southern Ocean was divided into two boxes to separate the two regions influenced by South American and Oceanian sources (Albani et al., 2014). In the same figure we show sites where LGM-Holocene export productivity changes were measured in marine sediment cores (Kohfeld et al., 2013, 2005; Kohfeld and Chase, 2011). Note that export productivity measured in marine sediment cores is influenced not only by aeolian dust deposition, but also by ocean stratification and circulation, sea-ice, terrestrial input etc. Here, we only consider the effect of dust.

2.2. cGENIE model simulations

We use the cGENIE Earth system model to project the impact on atmospheric CO_2 of regional heterogeneity in dust flux to the ocean surface, and using the results, create regression models to estimate how changing dust deposition drives variability in CO_2 with time (since the last glacial). The version of the cGENIE model we use is described in detail in the supplementary information, particularly with respect to how it represents the cycle of iron in the ocean, but is summarized as follows.

cGENIE is based on a 3-D frictional geostrophic ocean circulation model, coupled with a 2-D energy-moisture balance model of dynamic-thermodynamic sea-ice and atmosphere (see SI). We apply this on a 36×36 equal-area horizontal grid with 16 logarithmically spaced levels in ocean depth (Cao et al., 2009). The horizontal grid is spaced in increments of 10° longitude, while the latitude grid spacing is uniform in sine of latitude, meaning that cell size varies from ~3.2° at the Equator to 19.2° at the poles. The parameters controlling ocean/atmosphere/sea-ice dynamics and hence climate, are those used in (Cao et al., 2009).

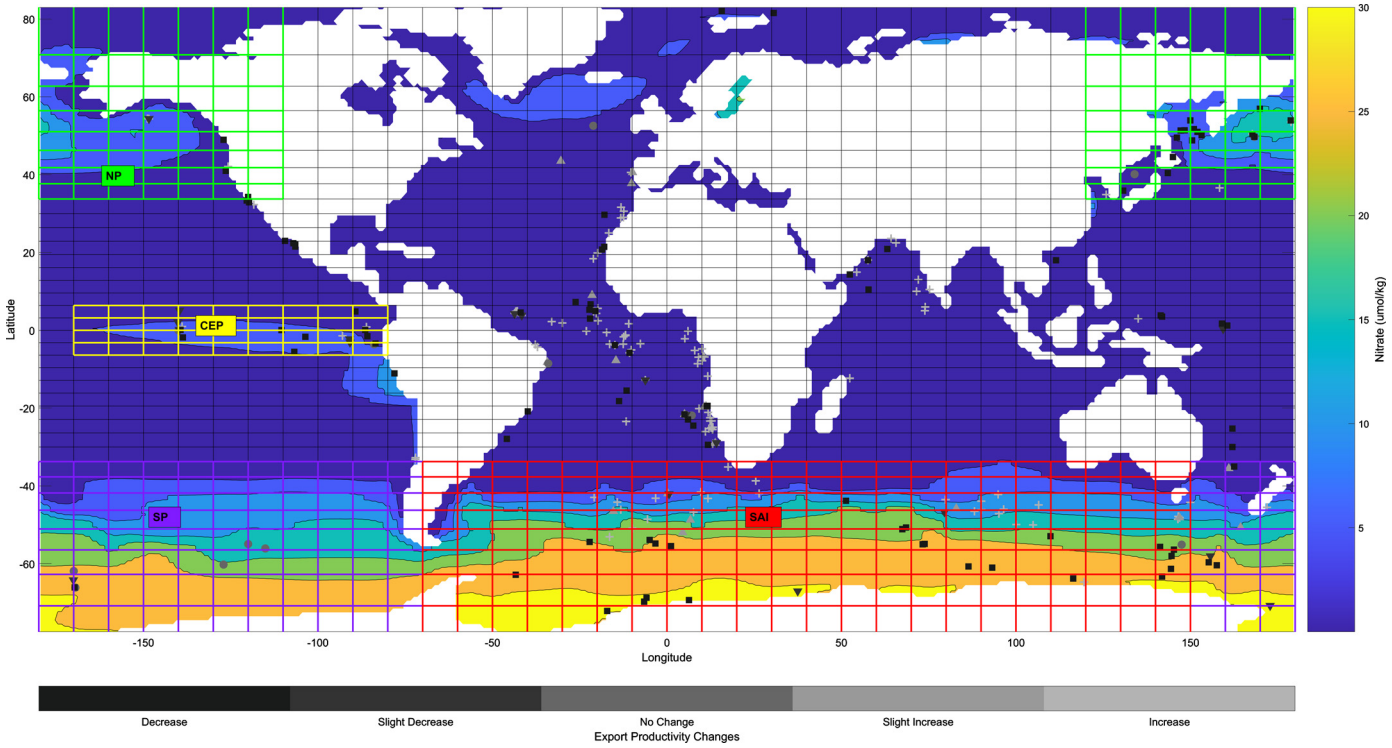

Fig. 1. World grid as used as input for the cGENIE model. Ocean color represents Holocene nitrate surface concentrations (Lambert et al., 2015) (right colorbar). The 4 main HNLC regions (SAI, SP, NP, CEP) are marked in color. The plus signs, upward-pointing triangles, circles, downward-pointing triangles, and squares represent LGM-Holocene export productivity increase, slight increase, no change, slight decrease, and decrease, respectively, measured in marine sediment cores (Kohfeld et al., 2013, 2005; Kohfeld and Chase, 2011) and color-coded in the bottom color bar (Albani et al., 2014; Lambert et al., 2015; Ohgaito et al., 2018; Sueyoshi et al., 2013; Takemura et al., 2009; Yukimoto et al., 2012). (For interpretation of the colors in the figure(s), the reader is referred to the web version of this article.)

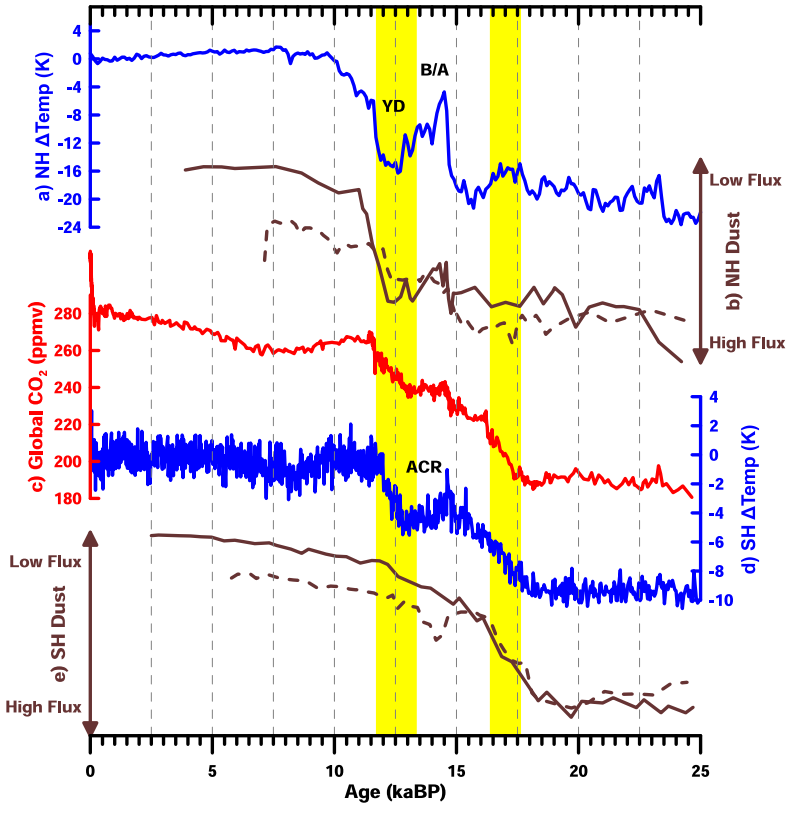

Fig. 2. a) Greenland ice-core temperature fluctuations (Masson-Delmotte et al., 2006). b) Aeolian dust deposition in the North Pacific (Serno et al., 2014) (full line) and the Equatorial Pacific (Jacobel et al., 2016) (dotted line). c) Global CO_2 concentrations from an Antarctic ice-core (Bereiter et al., 2015). d) Antarctic ice-core temperature fluctuations (Jouzel et al., 2007). e) Aeolian dust deposition in the South Atlantic (Anderson et al., 2014) (full line) and the South Pacific (Lamy et al., 2014) (dotted line).

Table 1
LGM dust forcing values (LGM - Holocene) summed over each region's area in kg/s. The excluded results from Fig. 4 (main text) are shown in gray. Negative values mean that the model simulated lower LGM dust deposition in that region than during the Holocene.

Region \ Dataset	Lambert	Albani	Takemura	MIROC ESM	MRI CGCM3	Ohgaito
Global	169129.2	121753.5	97309.0	136425.7	24889.0	291435.4
SAI	5863.5	22710.4	−55.4	−245.2	689.8	50482.1
SP	2067.5	393.6	4.0	−2.9	−18.7	727.1
NP	16076.2	11586.8	342.8	2657.9	1383.0	84155.0
CEP	231.0	93.2	112.0	172.6	21.9	124.1

For the marine carbon cycle, we utilize a dual, co-limited nutrient scheme consisting of phosphate and dissolved iron. The most pertinent facet of the cGENIE model iron cycle used in this study is the non-linear relationship between dust flux to the ocean surface, and the solubility of iron in that dust (see SI). This acts to smooth out the spatial heterogeneity in the dissolved iron flux to the ocean surface as compared to solid (dust) flux (SI Figure S1). Similarly, it also acts to reduce the impact (in terms of dissolved iron flux) of the differences between alternative dust reconstructions (SI Figure S2). Loss of dissolved Fe from the ocean occurs both through biological uptake (in a varying ratio with carbon), and through scavenging onto sinking particulate organic matter (as a function of both ambient dissolved Fe concentrations and the organic matter flux).

It should be noted that the aim of this study is to isolate the effect of dust on atmospheric CO_2 from the combined 'real world' effect of changes in dust, ocean circulation and stratification, sea-ice, temperature etc. between glacial and interglacial states. Hence our adoption of the PI-control conditions of (Cao et al., 2009). The only change we consider between experiments is in the spatial field of dust flux and calculate its attendant impact atmospheric CO_2. Our results therefore do not necessarily match productivity records from marine sediment cores whose variability is affected not only by dust, but also by a multitude of as yet, poorly constrained physical climate and potentially also biogeochemical, changes.

We considered six different estimates of paired Holocene and LGM dust fluxes: one based on paleoarchive measurement interpolation, and the other five based on the few Earth System Model simulations that include dust in their LGM simulations. They are hereafter respectively called "Lambert" (Lambert et al., 2015), "Albani" (Albani et al., 2014), "Takemura" (Takemura et al., 2009), "MIROC-ESM" (Sueyoshi et al., 2013), "MRI-CGCM3" (Yukimoto et al., 2012), and "Ohgaito" (Ohgaito et al., 2018) (Fig. 3). All dust flux fields were regridded (equal area) to a 36×36 grid to be used as input in cGENIE. Although the interpolated ("Lambert") dataset is based on paleoarchive data, the uncertainty for single points used in the interpolation can be large, and the values may not necessarily be more correct than a simulation, especially in regions with sparse coverage (Lambert et al., 2015). The LGM dust forcing values for each region and input dataset are shown in Table 1.

We performed spin-up simulations using the cGENIE Earth system model of 10,000 years, for the six Holocene dust fields, prescribing the atmospheric CO_2 concentrations at 278 ppmv throughout (10,000 years is sufficient for even the deep ocean to reach equilibrium). Sets of all control (Holocene) and increased dust simulations were then performed, again for 10,000 years each, and starting from the end of the spin-up experiments. The final atmospheric CO_2 concentration for each simulation was taken as the mean of the last 500 years of the simulation.

2.3. CO_2: dust relationship

In addition to the Holocene and LGM dust flux fields provided by the one data-based interpolation and five GCM simulations, we created eight intermediate flux fields between Holocene and LGM values - one set of 8 for each of these six initial flux field pairs (a total of 60 different global dust patterns). The new flux fields were spaced logarithmically between the Holocene and LGM boundary values to resolve possible higher fertilization sensitivity at lower dust levels. Finally, for each of the 8 intermediate flux fields plus glacial (and for each of the 6 different dust reconstructions), we allowed the dust to vary only in one of the HNLC regions (and repeated this for all 4 HNLC regions) and simulated the CO_2 drawdown. Hence, for each of the 6 dust reconstructions, we created 5 sets of dust pattern varying in 8 (intermediate) steps from Holocene to glacial – one in which dust varied globally, and 4 in which dust varied only in the HNLC regions. These results form the basis for estimating an empirical relationship between the amount of dust (area sum) deposited in a region and the atmospheric CO_2 response (SI Figure S5). For this we chose a 4-parameter exponential fit to accommodate both linear and exponential behavior.

In order to map CO_2 onto time using our regression functions, for each HNLC region, we selected a dust flux or dust flux proxy time series that covers the last glacial termination time span (Figure S6). For the SAI region we chose a dust flux dataset from the South Atlantic (Anderson et al., 2014), for the SP region a fine fraction dust flux record (Lamy et al., 2014), for the NP region a crustal ^{4}He record as a dust proxy (Serno et al., 2015), and for the CEP region a dust flux record (Jacobel et al., 2016). Although the dust fluxes (or dust proxy) in these time series are reconstructed at just a single point in the ocean, their relative variability can be expected to be representative of dust deposition variability over a wider region (in fact, choosing a different record in a region does not fundamentally influence the message of this study (SI Figure S7). We therefore scaled the maxima and minima of each time series to the maximum and minimum of the corresponding region's dust flux area sum from each dust dataset (i.e. the LGM and Holocene values of the 5 simulations and 1 interpolation). Now we apply the empirical CO_2: dust relationship to these scaled time series to obtain the timing of the CO_2 response to the changing dust deposition through the termination. The dust-CO_2 relationships yields the estimated CO_2 response to the amount of dust deposited in each region every 500 years during the termination (all four marine sediment dust proxy records have a higher resolution than 500 years during the termination). Since the CO_2:dust relationship is not linear, the time series of the CO_2 response will not necessarily have the same shape as the measured dust flux or proxy time series.

3. Results and discussion

The absolute LGM CO_2 reduction values compared to pre-industrial CO_2 for the change from Holocene to LGM for each dust flux dataset are listed in Table 2. The model-calculated range of CO_2 change for global-scale IF is between 12 and 29 ppmv, in agreement with previous studies (Kohfeld and Ridgwell, 2013; Köhler and Fischer, 2006; Lambert et al., 2015; Shaffer and Lambert, 2018). We then break this down and show in Fig. 4 the relative contribution to the global simulated IF CO_2 drawdown from changing dust fluxes into each individual region.

The SAI region is the largest contributor to the global total dust CO_2 sensitivity ($41 \pm 23\%$), but with a large spread across dust

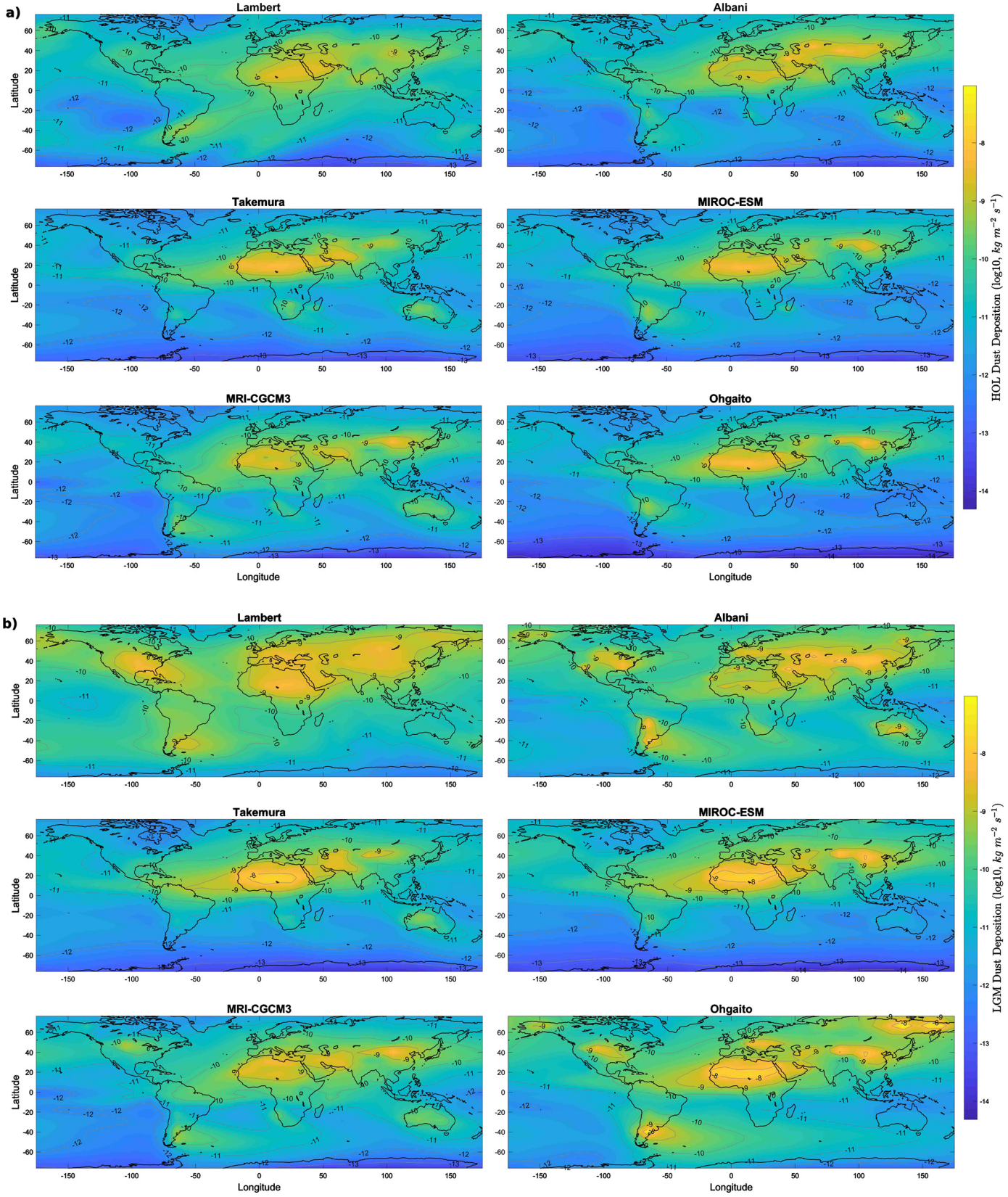

Fig. 3. a) Holocene (pre-industrial) and b) Last Glacial Maximum (21 kaBP) dust deposition fields used as forcing for the simulations (Albani et al., 2014; Lambert et al., 2015; Ohgaito et al., 2018; Sueyoshi et al., 2013; Takemura et al., 2009; Yukimoto et al., 2012).

Table 2
Absolute LGM-HOL atmospheric CO_2 concentration reduction in ppmv due to aeolian dust iron fertilization for all simulated regions and all input datasets. The excluded results from Fig. 4 are shown in gray.

Region \ Dataset	Lambert	Albani	Takemura	MIROC_ESM	MRI_CGCM3	Ohgaito
Global	16.6	26.7	16.0	20.3	8.9	33.1
SAI	5.7	15.2	−0.5	−1.2	1.0	20.2
SP	4.6	2.4	0.0	−0.1	−0.1	3.8
NP	5.1	8.4	1.1	5.5	2.5	8.2
CEP	0.7	0.6	0.9	1.2	0.2	1.0

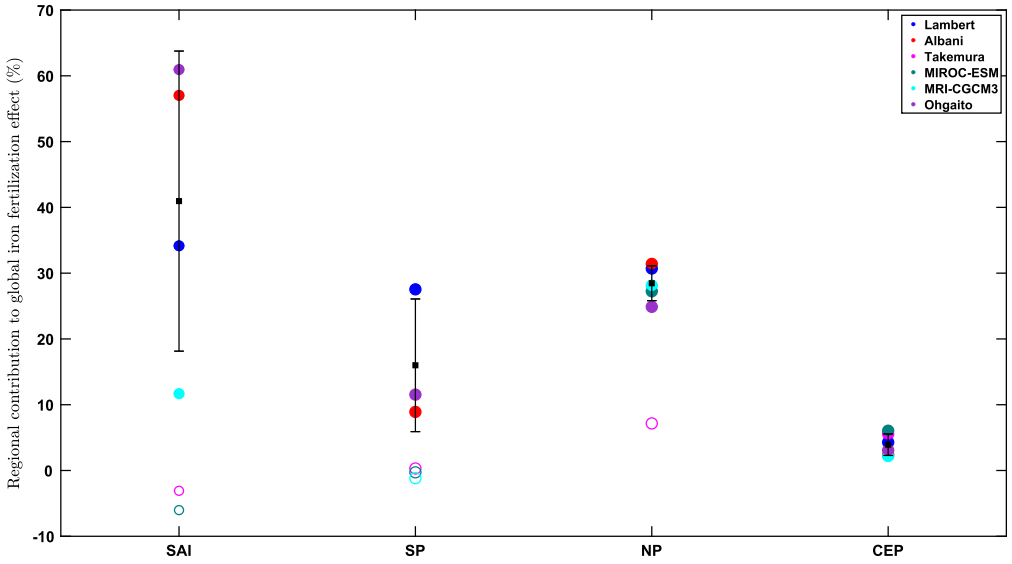

Fig. 4. Relative contribution of each HNLC region (South Atlantic and Indian, South Pacific, North Pacific, Central Eastern Pacific) to the atmospheric CO_2 changes in the global simulation for each dust dataset. Empty circles in SAI and SP were excluded due to missing representation of Patagonian and Oceanian glaciogenic emissions in these LGM simulations. The black square with error bars shows the mean and standard deviation of the not excluded results.

datasets. This spread is likely at least partly due to the absence of increased Patagonian LGM glaciogenic dust emissions in the Takemura and MIROC-ESM simulations. Since observations from Antarctic ice cores and south Atlantic marine sediment measurements show that Patagonian glaciogenic sources contributed most of the LGM dust (Anderson et al., 2014; Lambert et al., 2008), we omitted these results from the averaging statistics (excluded results are shown as an empty circle). The remaining spread is still large, however, reflecting the lack of knowledge about source emission changes in continental South America.

The SP region only accounts for 16 ± 10% of total CO_2 drawdown despite its large size. We attribute this more muted carbon cycle response to the relatively smaller LGM dust deposition increase in the SP region in comparison to the SAI (Lamy et al., 2014). In this region, we excluded the Takemura, MIROC-ESM, and MRI-CGCM2 simulations because none of these included the increased Australian and New Zealand LGM dust emissions measured in the SP (Chase et al., 2003; Lamy et al., 2014).

The contribution of the NP region amounts to 28 ± 3% of total CO_2 drawdown. Five of our results are in very close agreement between 25 and 30% of total drawdown. In contrast, the Takemura simulation indicates a contribution below 10%. This is due to the omission of Asian and Siberian glaciogenic dust sources in the Takemura simulation (Ohgaito et al., 2018). We have therefore also omitted the Takemura simulation from the NP statistics.

Finally, the results from all simulations agree on a low contribution of the CEP region of 4 ± 2% of the total IF CO_2 drawdown, in agreement with recent productivity estimates from marine sediment records (Costa et al., 2016).

We note that the sum of all regions' CO_2 drawdown will not necessarily equal the projected CO_2 drawdown in the global simulation. Iron fertilization increases nutrient utilization in high latitudes surface waters, which reduces the amount of nutrients transported to low latitudes by intermediate depth waters, reducing the tropical carbon export (Sarmiento et al., 2004). It is therefore likely that the simulation with global forcing includes interplay between regions that are not present in the simulations with forcing of single HNLC regions. Although our results confirm the Southern Ocean as the main region influencing CO_2 concentrations through iron fertilization, the contribution of the NP region is significant, and likely larger than the SP. Thus, the Northern Hemisphere may play an important dust-related role in glacial-interglacial atmospheric CO_2 variability.

To further elucidate the sensitivity of atmospheric CO_2 to dust, we tested eight intermediate proportions of Holocene vs. LGM dust fluxes in each region, in addition to the Holocene and LGM endmember simulations (see Methods section 2.3). Each set of ten simulations then forms the basis for a model-derived empirical relationship, linking the total amount of deposited dust in each HNLC region and the resulting change in atmospheric CO_2 (SI Fig. S5). Ridgwell (2003) suggested that atmospheric CO_2 would not react linearly to dust deposition, but rather be more sensitive to dust changes for small fluxes, when iron limitation is highest and small increases in dust can make a big difference. Indeed, small changes in dust fluxes tend to produce a linear relationship between CO_2 and dust, while larger changes seem to produce diminishing returns (SI Fig. S52). Using our set of empirical relationships, we then calculate time-varying histories across the deglaciation of potential CO_2 increase due to the reduction in dust flux and resulting weakening of the biological pump (Fig. 5). We have marked as dashed lines those datasets that were excluded in Fig. 4. In addition, we have added the global atmospheric CO_2 curve as a black dotted line for reference. In the SAI region, the CO_2 contribution rises relatively linearly in time, with slightly enhanced

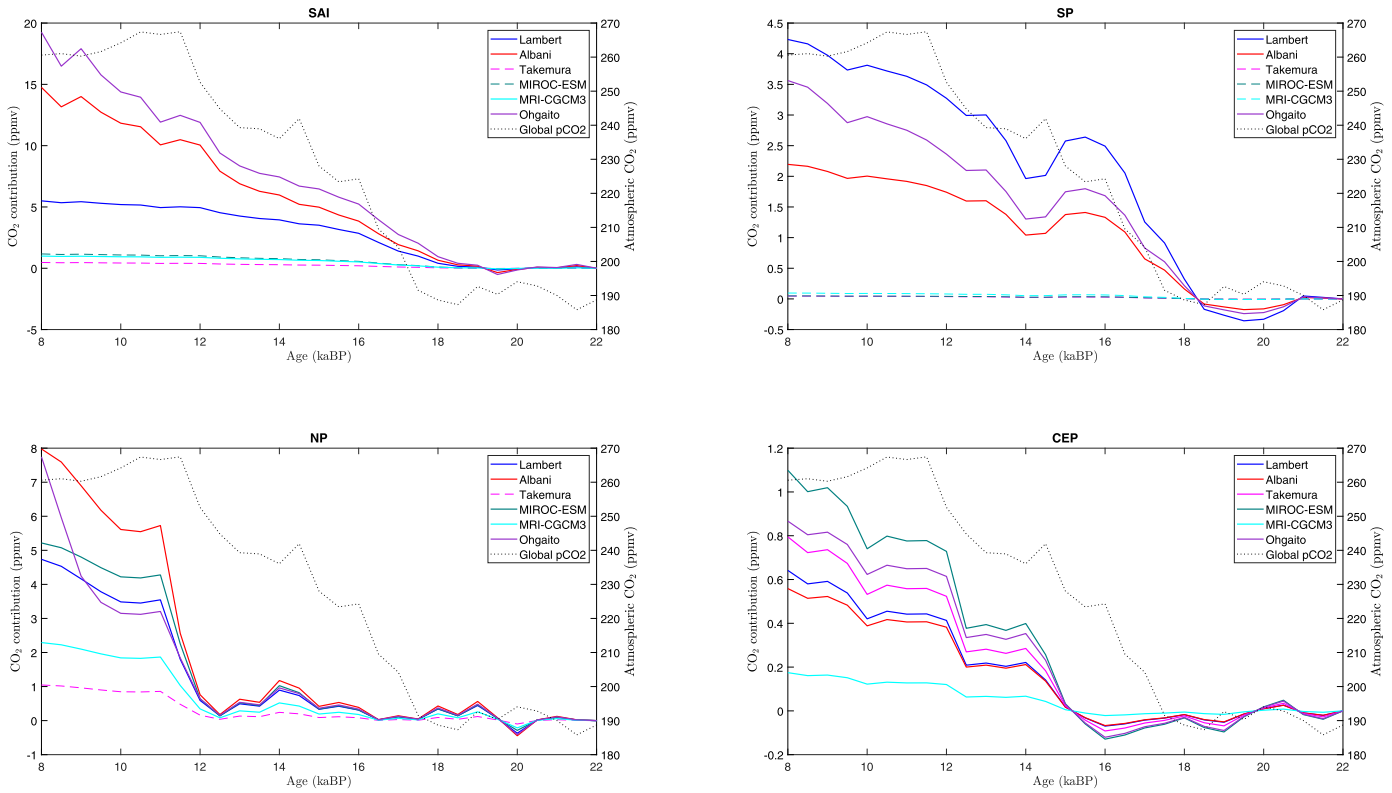

Fig. 5. The colored lines show the calculation of the CO_2 response to dust deposition based on the mathematical formula derived in Figure S5 and applied to the scaled measured dust flux time series in each HNLC region. Dashed lines in SAI, SP, and NP show the excluded results from Fig. 4. The global atmospheric CO_2 record is shown as a black dotted line plotted against the right axis.

rates of rise corresponding to both first and second observed CO_2 pulses. Although most of the SH dust reduction occurs early in the termination (Fig. 2), the high sensitivity of CO_2 at low dust flux values makes these small dust changes still relevant during the later stages of the termination. The changes in the SP region start very early and are more or less coeval with the first pulse. Due to their more northerly location than South America, Oceanian dust sources probably reached Holocene emission levels before the ACR and were not affected by the later termination temperature changes. This is consistent with glacier moraine data showing most LGM glaciers in New Zealand had collapsed by 16 kaBP (Alloway et al., 2007; Rother et al., 2014). This would have ended the supply of glaciogenic dust early in the termination due to pro-glacial lake formation (Sugden et al., 2009). In contrast, the NP region shows no sign of dust or CO_2 change during the early termination and the first pulse. Rather, the full impact of changing dust fluxes to this region occurs only during the second pulse. The main NP dust sources are the East Asian deserts, which shifted to an interglacial regime only in the late termination (Sun and An, 2005), keeping NP dust deposition at LGM levels during the early termination. The CO_2 response to dust reduction in the CEP region started during the ACR and continued throughout the second pulse. Assuming a mix of North American and Asian dust sources in this region (Albani et al., 2014), this suggests a possible collapse of North American dust sources during the ACR, coupled with the later effect of Asian sources.

For a total atmospheric CO_2 reduction of 18.5 ppmv from iron fertilization of the four HNLC regions during the termination (the medians of the non-discarded results in Fig. 4 summed over all four regions), atmospheric dust reduction contributed only 2.6 ppmv during the first pulse, but 5.6 ppmv during the second pulse, with the rest being contributed between and after the pulses. To put things into a wider perspective, we divide the termination into an early and a later half, with the division between them at 15 kaBP. Then, iron fertilization of the four HNLC regions reduced atmospheric CO_2 by 6.2 ppmv in the first period, and by 12.3 ppmv in the second one. We conclude that, although dust fluxes in the Southern Ocean fell very rapidly in the early termination, the major effect of lower iron fertilization of the oceans occurred in the second half of the termination, due to higher sensitivity of CO_2 changes at low dust flux levels when iron is strongly limited and to the late contribution in the Northern Hemisphere. Ocean destratification may have been the major reason for the first pulse of CO_2 with relatively little contribution from dust, while iron fertilization may have contributed more substantially to the second CO_2 pulse.

4. Conclusions

Using a carbon cycle centric EMIC we simulated the LGM changes in atmospheric CO_2 concentrations due to iron fertilization from aeolian dust deposition in four individual HNLC regions of the Earth's oceans, and derive empirical relationships between the amount of deposited dust and atmospheric CO_2 changes for each region. Overall, our findings confirm the dominant role of the Southern Ocean for iron fertilization, but point to a possibly greater role of the North Pacific in deglacial atmospheric CO_2 rise and climate change than generally appreciated. We show that although SH dust changes occurred early in the termination, the major effect of global aeolian iron fertilization on atmospheric CO_2 was during the second half of the termination. In this study, we isolated the effect of aeolian dust on surface ocean iron fertilization and CO_2 drawdown. In combination with other such studies that quantify different effects (ocean circulation, sea-ice, terrestrial input etc.) it may be possible in the future to untangle the various contributions from different effects to the total signal recorded in

marine sediments. Our paleo-derived sensitivity of the North Pacific to iron fertilization also has implications for future global iron cycle impacts and feedbacks on atmospheric CO_2. Desertification in China is accelerating due to climate change (Wang et al., 2008), but dust storm frequency is decreasing (Wu et al., 2018), which could affect CO_2 drawdown in the North Pacific.

CRediT authorship contribution statement

Fabrice Lambert: Conceptualization, Data curation, Formal analysis, Funding acquisition, Investigation, Methodology, Project administration, Resources, Software, Supervision, Visualization, Writing – original draft. **Natalia Opazo:** Formal analysis, Software. **Andy Ridgwell:** Formal analysis, Investigation, Resources, Software, Writing – review & editing. **Gisela Winckler:** Conceptualization, Writing – review & editing. **Frank Lamy:** Conceptualization, Writing – review & editing. **Gary Shaffer:** Writing – review & editing. **Karen Kohfeld:** Conceptualization, Writing – review & editing. **Rumi Ohgaito:** Writing – review & editing. **Samuel Albani:** Writing – review & editing. **Ayako Abe-Ouchi:** Writing – review & editing.

Declaration of competing interest

The authors declare that they have no known competing financial interests or personal relationships that could have appeared to influence the work reported in this paper.

Acknowledgements

This work was funded by the ANID/Millennium Science Initiative/Millennium Nucleus Paleoclimate NCN17_079. FL acknowledges support from projects ANID/Fondecyt 1191223 and ANID/Fondap 15110009. GS acknowledges support from project ANID/Fondecyt 1190230. RO acknowledges support from the Integrated Research Program for Advancing Climate Models (TOUGOU programme) grant JPMXD0717935715 from the Ministry of Education, Culture, Sports, Science and Technology (MEXT), Japan. The GCM simulations by RO were conducted on the Earth Simulator of JAMSTEC. AR acknowledges support from NSF under grant number 1736771. The cGENIE simulations were run on the computing cluster facility of AR at UCRiverside. KK acknowledges funding from a Natural Sciences and Engineering Research Council Canada Research Chairs Award.

Appendix A. Supplementary material

Supplementary material related to this article can be found online at https://doi.org/10.1016/j.epsl.2020.116675.

References

Albani, S., Mahowald, N.M., Perry, A.T., Scanza, R.A., Zender, C.S., Heavens, N.G., Maggi, V., Kok, J.F., Otto-Bliesner, B.L., 2014. Improved dust representation in the community atmosphere model. J. Adv. Model. Earth Syst. 6, 541–570. https://doi.org/10.1002/2013MS000279.

Alloway, B.V., Lowe, D.J., Barrell, D.J.A., Newnham, R.M., Almond, P.C., Augustinus, P.C., Bertler, N.A.N., Carter, L., Litchfield, N.J., McGlone, M.S., Shulmeister, J., Vandergoes, M.J., Williams, P.W., 2007. Towards a climate event stratigraphy for New Zealand over the past 30 000 years (NZ-INTIMATE project). J. Quat. Sci. 22, 9–35. https://doi.org/10.1002/jqs.1079.

Anderson, R.F., Barker, S., Fleisher, M., Gersonde, R., Goldstein, S.L., Kuhn, G., Mortyn, P.G., Pahnke, K., Sachs, J.P., 2014. Biological response to millennial variability of dust and nutrient supply in the Subantarctic South Atlantic Ocean. Philos. Trans. R. Soc. A, Math. Phys. Eng. Sci. 372. https://doi.org/10.1098/rsta.2013.0054.

Bereiter, B., Eggleston, S., Schmitt, J., Nehrbass-Ahles, C., Stocker, T.F., Fischer, H., Kipfstuhl, S., Chappellaz, J., 2015. Revision of the EPICA Dome C CO2 record from 800 to 600 kyr before present. Geophys. Res. Lett. 42, 542–549. https://doi.org/10.1002/2014GL061957.

Cao, L., Eby, M., Ridgwell, A., Caldeira, K., Archer, D., Ishida, A., Joos, F., Matsumoto, K., Mikolajewicz, U., Mouchet, A., Orr, J.C., Plattner, G.-K., Schlitzer, R., Tokos, K., Totterdell, I., Tschumi, T., Yamanaka, Y., Yool, A., 2009. The role of ocean transport in the uptake of anthropogenic CO2. Biogeosciences 6, 375–390. https://doi.org/10.5194/bg-6-375-2009.

Chase, Z., Anderson, R.F., Fleisher, M.Q., Kubik, P.W., 2003. Accumulation of biogenic and lithogenic material in the Pacific sector of the Southern Ocean during the past 40,000 years. Deep-Sea Res., Part 2, Top. Stud. Oceanogr. 50, 799–832. https://doi.org/10.1016/S0967-0645(02)00595-7.

Chikamoto, M.O., Abe-Ouchi, A., Oka, A., Ohgaito, R., Timmermann, A., 2012. Quantifying the ocean's role in glacial CO2 reductions. Clim. Past 8, 545–563. https://doi.org/10.5194/cp-8-545-2012.

Chowdhry Beeman, J., Gest, L., Parrenin, F., Raynaud, D., Fudge, T.J., Buizert, C., Brook, E.J., 2019. Antarctic temperature and CO2: near-synchrony yet variable phasing during the last deglaciation. Clim. Past 15, 913–926. https://doi.org/10.5194/cp-15-913-2019.

Costa, K.M., McManus, J.F., Anderson, R.F., Ren, H., Sigman, D.M., Winckler, G., Fleisher, M.Q., Marcantonio, F., Ravelo, A.C., 2016. No iron fertilization in the equatorial Pacific Ocean during the last ice age. Nature 529, 519–522. https://doi.org/10.1038/nature16453.

Fischer, H., Schmitt, J., Lüthi, D., Stocker, T.F., Tschumi, T., Parekh, P., Joos, F., Köhler, P., Völker, C., Gersonde, R., Barbante, C., Le Floch, M., Raynaud, D., Wolff, E., 2010. The role of Southern Ocean processes in orbital and millennial CO2 variations – a synthesis. Quat. Sci. Rev. 29, 193–205. https://doi.org/10.1016/j.quascirev.2009.06.007.

Francois, R., Altabet, M., Yu, E., Sigman, D., Bacon, M., Frank, M., Bohrmann, G., Bareille, G., Labeyrie, L., 1997. Contribution of Southern Ocean surface-water stratification to low atmospheric CO2 concentrations during the last glacial period. Nature 389, 929–935.

Hain, M.P., Sigman, D.M., Haug, G.H., 2014. The biological pump in the past. In: Holland, H., Turekian, K. (Eds.), Treatise on Geochemistry. Elsevier, pp. 485–517.

Jacobel, A.W., McManus, J.F., Anderson, R.F., Winckler, G., 2016. Large deglacial shifts of the Pacific intertropical convergence zone. Nat. Commun. 7, 1–7. https://doi.org/10.1038/ncomms10449.

Jouzel, J., Masson-Delmotte, V., Cattani, O., Dreyfus, G., Falourd, S., Hoffmann, G., Minster, B., Nouet, J., Barnola, J.M., Chappellaz, J., Fischer, H., Gallet, J.C., Johnsen, S., Leuenberger, M., Loulergue, L., Luethi, D., Oerter, H., Parrenin, F., Raisbeck, G., Raynaud, D., Schilt, A., Schwander, J., Selmo, E., Souchez, R., Spahni, R., Stauffer, B., Steffensen, J.P., Stenni, B., Stocker, T.F., Tison, J.L., Werner, M., Wolff, E.W., 2007. Orbital and millennial Antarctic climate variability over the past 800,000 years. Science 80 (317), 793–796. https://doi.org/10.1126/science.1141038.

Kohfeld, K.E., Chase, Z., 2011. Controls on deglacial changes in biogenic fluxes in the North Pacific Ocean. Quat. Sci. Rev. 30, 3350–3363. https://doi.org/10.1016/J.QUASCIREV.2011.08.007.

Kohfeld, K.E., Graham, R.M., de Boer, A.M., Sime, L.C., Wolff, E.W., Le Quéré, C., Bopp, L., 2013. Southern hemisphere westerly wind changes during the last glacial maximum: paleo-data synthesis. Quat. Sci. Rev. 68, 76–95. https://doi.org/10.1016/j.quascirev.2013.01.017.

Kohfeld, K.E., Le Quéré, C., Harrison, S.P., Anderson, R.F., 2005. Role of marine biology in glacial-interglacial CO2 cycles. Science 80 (308), 74–78. https://doi.org/10.1126/science.1105375.

Kohfeld, K.E., Ridgwell, A., 2013. Glacial-interglacial variability in atmospheric CO2. In: Surface Ocean-Lower Atmosphere Processes. American Geophysical, Union, pp. 251–286.

Köhler, P., Fischer, H., 2006. Simulating low frequency changes in atmospheric CO2 during the last 740 000 years. Clim. Past 2, 57–78. https://doi.org/10.5194/cp-2-57-2006.

Lambert, F., Delmonte, B., Petit, J., Bigler, M., Kaufmann, P., Hutterli, M., Stocker, T., Ruth, U., Steffensen, J., Maggi, V., 2008. Dust-climate couplings over the past 800,000 years from the EPICA Dome C ice core. Nature 452, 616–619. https://doi.org/10.1038/nature06763.

Lambert, F., Tagliabue, A., Shaffer, G., Lamy, F., Winckler, G., Farias, L., Gallardo, L., De Pol-Holz, R., 2015. Dust fluxes and iron fertilization in Holocene and last glacial maximum climates. Geophys. Res. Lett. 42, 6014–6023. https://doi.org/10.1002/2015GL064250.

Lamy, F., Gersonde, R., Winckler, G., Esper, O., Jaeschke, A., Kuhn, G., Ullermann, J., Martinez-Garcia, A., Lambert, F., Kilian, R., 2014. Increased dust deposition in the Pacific Southern Ocean during glacial periods. Science 343, 403–407. https://doi.org/10.1126/science.1245424.

Lisiecki, L.E., Raymo, M.E., 2005. A Pliocene-Pleistocene stack of 57 globally distributed benthic $\delta^{18}O$ records. Paleoceanography 20, 1–17. https://doi.org/10.1029/2004PA001071.

Lohmann, U., Feichter, J., 2005. Global indirect aerosol effects: a review. Atmos. Chem. Phys. 5, 715–737. https://doi.org/10.5194/acp-5-715-2005.

Martin, J.H., Gordon, R.M., Fitzwater, S.E., 1991. The case for iron. Limnol. Oceanogr. 36, 1793–1802.

Martínez-Botí, M.A., Marino, G., Foster, G.L., Ziveri, P., Henehan, M.J., Rae, J.W.B., Mortyn, P.G., Vance, D., 2015. Boron isotope evidence for oceanic carbon dioxide leakage during the last deglaciation. Nature 518, 219–222. https://doi.org/10.1038/nature14155.

Masson-Delmotte, V., Dreyfus, G., Braconnot, P., Johnsen, S., Jouzel, J., Kageyama, M., Landais, A., Loutre, M.-F., Nouet, J., Parrenin, F., Raynaud, D., Stenni, B., Tuenter, E., 2006. Past temperature reconstructions from deep ice cores: relevance for future climate change. Clim. Past 2, 145–165. https://doi.org/10.5194/cpd-2-399-2006.

Monnin, E., Indermuhle, A., Dallenbach, A., Fluckiger, J., Stauffer, B., Stocker, T.F., Raynaud, D., Barnola, J., 2001. Atmospheric CO2 over the last glacial termination. Science 80 (291), 112–114.

Ohgaito, R., Abe-Ouchi, A., O'Ishi, R., Takemura, T., Ito, A., Hajima, T., Watanabe, S., Kawamiya, M., 2018. Effect of high dust amount on surface temperature during the last glacial maximum: a modelling study using MIROC-ESM. Clim. Past 14, 1565–1581. https://doi.org/10.5194/cp-14-1565-2018.

Pourmand, A., Marcantonio, F., Schulz, H., 2004. Variations in productivity and eolian fluxes in the northeastern Arabian Sea during the past 110 ka. Earth Planet. Sci. Lett. 221, 39–54. https://doi.org/10.1016/S0012-821X(04)00109-8.

Ridgwell, A.J., 2003. Implications of the glacial CO2 "iron hypothesis" for quaternary climate change. Geochem. Geophys. Geosyst. 4, 1–10. https://doi.org/10.1029/2003GC000563.

Rother, H., Fink, D., Shulmeister, J., Mifsud, C., Evans, M., Pugh, J., 2014. The early rise and late demise of New Zealand's last glacial maximum. Proc. Natl. Acad. Sci. USA 111, 11630–11635. https://doi.org/10.1073/pnas.1401547111.

Sarmiento, J.L., Gruber, N., Brzezinski, M.A., Dunne, J.P., 2004. High-latitude controls of thermocline nutrients and low latitude biological productivity. Nature 427, 56–60. https://doi.org/10.1038/nature02127.

Serno, S., Winckler, G., Anderson, R.F., Hayes, C.T., McGee, D., Machalett, B., Ren, H., Straub, S.M., Gersonde, R., Haug, G.H., 2014. Eolian dust input to the subarctic North Pacific. Earth Planet. Sci. Lett. 387, 252–263. https://doi.org/10.1016/j.epsl.2013.11.008.

Serno, S., Winckler, G., Anderson, R.F., Maier, E., Ren, H., Gersonde, R., Haug, G.H., 2015. Comparing dust flux records from the subarctic North Pacific and Greenland: implications for atmospheric transport to Greenland and for the application of dust as a chronostratigraphic tool. Paleoceanography 30, 583–600. https://doi.org/10.1002/2014PA002748.

Shaffer, G., Lambert, F., 2018. In and out of glacial extremes by way of dust-climate feedbacks. Proc. Natl. Acad. Sci. USA 115, 2026–2031. https://doi.org/10.1073/pnas.1708174115.

Shakun, J.D., Clark, P.U., He, F., Marcott, S.a, Mix, A.C., Liu, Z., Otto-Bliesner, B., Schmittner, A., Bard, E., 2012. Global warming preceded by increasing carbon dioxide concentrations during the last deglaciation. Nature 484, 49–54. https://doi.org/10.1038/nature10915.

Shoenfelt, E.M., Winckler, G., Lamy, F., Anderson, R.F., Bostick, B.C., 2018. Highly bioavailable dust-borne iron delivered to the Southern Ocean during glacial periods. Proc. Natl. Acad. Sci. 201809755. https://doi.org/10.1073/pnas.1809755115.

Sigman, D.M., Boyle, E.A., 2000. Glacial/interglacial variations in atmospheric carbon dioxide. Nature 407, 859–869. https://doi.org/10.1038/35038000.

Sueyoshi, T., Ohgaito, R., Yamamoto, A., Chikamoto, M.O., Hajima, T., Okajima, H., Yoshimori, M., Abe, M., O'ishi, R., Saito, F., Watanabe, S., Kawamiya, M., Abe-Ouchi, A., 2013. Set-up of the PMIP3 paleoclimate experiments conducted using an Earth system model, MIROC-ESM. Geosci. Model Dev. 6, 819–836. https://doi.org/10.5194/gmd-6-819-2013.

Sugden, D.E., McCulloch, R.D., Bory, A.J.-M., Hein, A.S., 2009. Influence of Patagonian glaciers on Antarctic dust deposition during the last glacial period. Nat. Geosci. 2, 281–285. https://doi.org/10.1038/ngeo474.

Sun, Y., An, Z., 2005. Late Pliocene-Pleistocene changes in mass accumulation rates of eolian deposits on the central Chinese Loess Plateau. J. Geophys. Res., Atmos. 110, 1–8. https://doi.org/10.1029/2005JD006064.

Tagliabue, A., Bowie, A.R., Boyd, P.W., Buck, K.N., Johnson, K.S., Saito, M.A., 2017. The integral role of iron in ocean biogeochemistry. Nature 543, 51–59. https://doi.org/10.1038/nature21058.

Takemura, T., Egashira, M., Matsuzawa, K., Ichijo, H., O'ishi, R., Abe-Ouchi, A., 2009. A simulation of the global distribution and radiative forcing of soil dust aerosols at the last glacial maximum. Atmos. Chem. Phys. 9, 3061–3073. https://doi.org/10.5194/acp-9-3061-2009.

Tegen, I., Lacis, A.A., Fung, I., 1996. The influence on climate forcing of mineral aerosols from disturbed soils. Nature 380, 419–422. https://doi.org/10.1038/380419a0.

Wang, X., Chen, F., Hasi, E., Li, J., 2008. Desertification in China: an assessment. Earth-Sci. Rev. 88, 188–206. https://doi.org/10.1016/J.EARSCIREV.2008.02.001.

Watson, A.J., Bakker, D.C., Ridgwell, A.J., Boyd, P.W., Law, C.S., 2000. Effect of iron supply on Southern Ocean CO2 uptake and implications for glacial atmospheric CO2. Nature 407, 730–733. https://doi.org/10.1038/35037561.

Wu, C., Lin, Z., Liu, X., Li, Y., Lu, Z., Wu, M., 2018. Can climate models reproduce the decadal change of dust aerosol in East Asia? Geophys. Res. Lett. 45, 9953–9962. https://doi.org/10.1029/2018GL079376.

Yamamoto, A., Abe-Ouchi, A., Ohgaito, R., Ito, A., Oka, A., 2019. Glacial CO2 decrease and deep-water deoxygenation by iron fertilization from glaciogenic dust. Clim. Past 15, 981–996. https://doi.org/10.5194/cp-15-981-2019.

Yukimoto, S., Adachi, Y., Hosaka, M., Sakami, T., Yoshimura, H., Hirabara, M., Tanaka, T.Y., Shindo, E., Tsujino, H., Deushi, M., Mizuta, R., Yabu, S., Obata, A., Nakano, H., Koshiro, T., Ose, T., Kitoh, A., 2012. A new global climate model of the meteorological research institute: MRI-CGCM3. J. Meteorol. Soc. Jpn. 90A, 23–64. https://doi.org/10.2151/jmsj.2012-A02.